

Divergence error based p -adaptive discontinuous Galerkin solution of time-domain Maxwell's equations

Apurva Tiwari^{*,1} and Avijit Chatterjee¹

¹*Department of Aerospace Engineering, Indian Institute of Technology Bombay, India*

1 Abstract

A p -adaptive discontinuous Galerkin time-domain method is developed to obtain high-order solutions to electromagnetic scattering problems. A novel feature of the proposed method is the use of divergence error to drive the p -adaptive method. The nature of divergence error is explored and that it is a direct consequence of the act of discretization is established. Its relation with relative truncation error is formed which enables the use of divergence error as an inexpensive proxy to truncation error. Divergence error is used as an indicator to dynamically identify and assign spatial operators of varying accuracy to substantial regions in the computational domain. This results in a reduced computational cost than a comparable discontinuous Galerkin time-domain solution using uniform degree piecewise polynomial bases throughout.

Keywords: Discontinuous Galerkin; Divergence error; Higher-order; Time-domain; Maxwell's equations

2 Introduction

A variety of physical phenomena are modelled as systems of partial differential equations that admit divergence-free solutions. In some of these, like the incompressible Euler and Navier-Stokes equations, this condition of the solution being divergence-free is enforced explicitly. In certain other systems like the time-domain Maxwell's equations, the usual practice is to incorporate the solenoidal condition within the evolution equations, combined with the

^{*}Corresponding author.

Email addresses: apurva.t@aero.iitb.ac.in (A. Tiwari), avijit@aero.iitb.ac.in (A. Chatterjee)

requirement that the initial conditions be solenoidal. It relies on the reasoning that if field variables are initially divergence-free, they remain so when evolved in time using the first order div-curl equations. Not all numerical schemes try to satisfy the solenoidal condition.

The finite difference time domain (FDTD) method proposed by Yee [1] to solve the time-domain Maxwell's equations, satisfies the divergence-free condition by design. It uses a grid where different components of the field variables are computed at staggered spatial and temporal points. Assuming zero initial conditions, the time derivative of the net flux from the surface of a Yee cell remains a constant zero, satisfying Gauss' Law [2]. Advancements in higher order Godunov schemes for problems in computational electromagnetism (CEM) gave rise to the finite volume time domain (FVTD) [3] and discontinuous Galerkin time domain (DGTd) methods [4]. These schemes do not account for the divergence constraint in the time domain Maxwell system. In literature, there are various approaches to meet the constraint imposed by Gauss' law. A divergence cleaning step is often added that solves a Poisson equation for a correction potential. Assous [5] used a constrained variational formulation of Maxwell's equations and applied a penalization technique. In [6], Munz et. al. reformulated the constrained Maxwell's equations and introduced a coupling term into Gauss' law, rendering a perfectly hyperbolic system of equations. This made for a natural extension of the explicit methods for Maxwell's equations to a purely hyperbolic system. In DGTd, with standard piecewise polynomial spaces used and no dedicated measures for constraint preservation taken, it is observed that global divergence errors are k th order small when using polynomial bases of degree k to represent the solution [7]. DG schemes based on locally divergence-free bases [7, 8] and globally divergence constraint preserving methods, for hyperbolic conservation laws [9] and for ideal magnetohydrodynamics (MHD) [10, 11] have been proposed.

Another aspect is that divergence errors accruing in conservative higher-order formulations do not significantly impact the overall accuracy of the solution [6, 12] and are often disregarded in practice. In [12], Cioni et. al used a mixed finite volume/finite element method to show that divergence error, despite being linked to the accuracy of the solver and the underlying discretization, does not hamper the formal accuracy of the solution.

In this paper, we propose another point of view, that of constructively using this error in divergence to improve spatial accuracy, rather than of either ignoring or eliminating the naturally occurring divergence error in conservative, non FDTD frameworks for solving the time domain Maxwell's equations. We establish that relative divergence and relative truncation errors in DGTd methods are related and propose that divergence error can be used as an effective truncation error indicator. Since solving the evolution equations does not decrease divergence error in computations, it constantly tracks truncation error. The proposed divergence based error indicator may be utilized to drive adaptive methods that assign spatial operators of varying accuracy in the computational domain, with the motive of achieving desired levels of accuracy using fewer degrees of freedom (DOFs).

We begin with the transverse magnetic (TM) mode of the time-domain Maxwell's equations to formulate the formal relation between the relative truncation error in the residual appearing in the semi-discrete system and the evolution and propagation of the associated relative divergence errors. Here, relative refers to the difference between quantities computed using different discretizations [13]. We extend this definition to incorporate it in a p -adaptive DGTD framework. Different levels of discretizations are obtained by operators formed using polynomial bases of varying degrees. The formulated relation is applied on plane wave solutions and the resultant simplified expressions obtained, are verified by solving canonical problems using DGTD. The correlation between discretization error in solutions and their divergence is also shown with numerical examples. Numerical solutions including scattering off circular cylinders and a semi-open cavity, using a simple p -adaptive algorithm based on divergence error are presented.

3 Discontinuous Galerkin time domain method

This section briefly outlines the discontinuous Galerkin time domain method. A detailed account can be found in the text by Hesthaven et. al. [4], part of which is presented in this section.

Consider a system of hyperbolic conservation laws,

$$\frac{\partial \mathbf{u}}{\partial t} + \nabla \cdot \mathcal{F} = \mathbf{s} \quad (1)$$

where, $\mathbf{u} = [q_1, \dots, q_n]^T$ is a vector of conserved variables, \mathcal{F} is the flux tensor depending on q , and s is a source term. This system is representative, among others, of the Maxwell's curl equations. For instance, consider the vector components in the 2D TM_z mode, for which

$$\mathbf{u} = \begin{pmatrix} B_x \\ B_y \\ D_z \end{pmatrix}, \quad \mathbf{f} = \begin{pmatrix} 0 \\ -D_z/\epsilon \\ -B_y/\mu \end{pmatrix}, \quad \mathbf{g} = \begin{pmatrix} D_z/\epsilon \\ 0 \\ B_x/\mu \end{pmatrix}, \quad \mathbf{s} = \begin{pmatrix} 0 \\ 0 \\ -J_{iz} \end{pmatrix}. \quad (2)$$

and in the 2D TE_z mode given by,

$$\mathbf{u} = \begin{pmatrix} B_z \\ D_x \\ D_y \end{pmatrix}, \quad \mathbf{f} = \begin{pmatrix} D_z/\epsilon \\ 0 \\ B_z/\mu \end{pmatrix}, \quad \mathbf{g} = \begin{pmatrix} -D_x/\epsilon \\ -B_z/\mu \\ 0 \end{pmatrix}, \quad \mathbf{s} = \begin{pmatrix} 0 \\ -J_{ix} \\ -J_{iy} \end{pmatrix}. \quad (3)$$

with $\mathcal{F} = [\mathbf{f}, \mathbf{g}]$ as corresponding flux vectors in the x and y directions, along with constituent relations $\mathbf{B} = \mu \mathbf{H}$, $\mathbf{D} = \epsilon \mathbf{E}$. The spatial domain Ω is triangulated as K elements, $\Omega \simeq \Omega_h = \bigcup_{k=1}^K \mathbf{D}^k$ and its boundary $\partial\Omega_h$, where \mathbf{D}^k is a straight-sided triangle with the triangulation assumed to be geometrically conforming.

The solution \mathbf{u} is approximated as \mathbf{u}_h and expressed locally as a polynomial expansion using local polynomial bases of order p , defined on element \mathbf{D}^k . The

global solution is given by,

$$\mathbf{u}(\mathbf{x}, t) \simeq \mathbf{u}_h(\mathbf{x}, t) = \bigoplus_{k=1}^K \mathbf{u}_{h,p}^k(\mathbf{x}, t) \in \mathbf{V}_h = \bigoplus_{k=1}^K \{\psi_n(\mathbf{D}^k)\}_{n=1}^{N_p} \quad (4)$$

Here $\psi_n(\mathbf{D}^k)$ is a two-dimensional polynomial basis defined on element \mathbf{D}^k . \mathbf{V}_h is a space of piecewise polynomial functions on Ω_h . It is required that the residual be orthogonal to all test functions in \mathbf{V}_h , and the choice that the test functions and the basis functions span the same space leads to the Galerkin scheme.

$$\int_{\Omega} \left(\frac{\partial \mathbf{u}_h}{\partial t} + \frac{\partial \mathbf{f}_h}{\partial x} + \frac{\partial \mathbf{g}_h}{\partial y} \right) \psi_n(\mathbf{x}) = 0; \quad \forall \psi_h \in \mathbf{V}_h \quad (5)$$

Here, we have assumed \mathbf{s} to be zero, *i.e.* free space, for ease of explanation with minimal loss of generality. A component u of the solution, is locally expressed as a p -th order polynomial expansion $u_{h,p}^k$,

$$\mathbf{x} \in \mathbf{D}^k : u_{h,p}^k(\mathbf{x}, t) = \sum_{i=1}^{N_p} u_{h,p}^k(\mathbf{x}_i, t) \ell_i^k(\mathbf{x}). \quad (6)$$

Here, $N_p = (p+1)(p+2)/2$, is the number of nodes in element \mathbf{D}^k . $\ell_i^k(\mathbf{x})$ is a p -th order multidimensional Lagrange polynomial, based on nodes \mathbf{x}_i on \mathbf{D}^k . Note that the local order p is allowed to vary across elements, *i.e.* $p = p(k)$. Simple manipulation of eq. (5) leads to the local statements,

$$\int_{\mathbf{D}^k} \left(\frac{\partial \mathbf{u}_h^k}{\partial t} + \nabla \cdot \mathcal{F}_h^k \right) \ell_i^k(\mathbf{x}) d\mathbf{x} = \int_{\partial \mathbf{D}^k} \hat{\mathbf{n}} \cdot [\mathcal{F}_h^k - \mathcal{F}^*] \ell_i^k(\mathbf{x}) d\mathbf{x}, \quad (7)$$

where $\hat{\mathbf{n}}$ is the local outward pointing normal to the element boundary $\partial \mathbf{D}^k$. Eq. (7) is referred to as the strong form, obtained by integrating by parts eq. (5) twice. \mathcal{F}^* is the upwind flux,

$$\hat{\mathbf{n}} \cdot (\mathcal{F}_h^k - \mathcal{F}^*) = \frac{1}{2} \begin{pmatrix} \hat{n}_y [E_z] + \hat{n}_x (\mathbf{H}) - [H_x] \\ -\hat{n}_x [E_z] + \hat{n}_y (\mathbf{H}) - [H_y] \\ \hat{n}_y [H_x] - \hat{n}_x [H_y] - [E_z] \end{pmatrix}, \quad (8)$$

where the following notation is used,

$$[q] = q^- - q^+ = \hat{\mathbf{n}} \cdot \langle q \rangle.$$

Here, q^- and q^+ are limits of the values of q at the interface from the interior and exterior of an element.

We now briefly discuss implementation considerations. Computing the numerical flux needs knowledge of the corresponding neighbours of each node, the u^+ as referred to in this section. To accommodate a variation of p across elements, it is imperative to address situations like the one shown in fig. 1. Neighbouring elements are at different levels of spatial accuracy and therefore

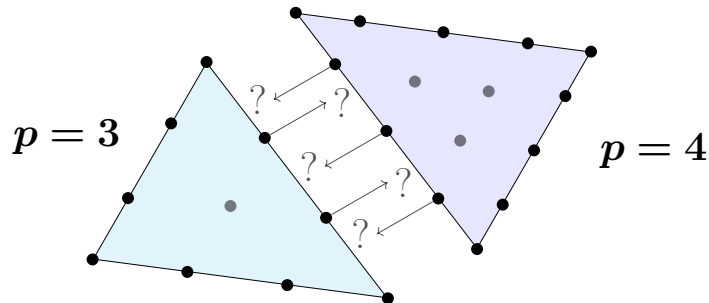


Figure 1: “Misaligned” neighbouring nodes at common edges in a p -variable nodal DG framework

have an unequal number of nodes representing the solution in each element. In a nodal DG setup, this leads to the problem of finding the limit of u at the interface from the exterior. Here, we resort to a polynomial interpolation [14] of the data using eq. (6), from a neighbouring element to the nodes required. So in fig. 1, interpolation of the solution in the bottom triangle, to nodes on the common edge between its neighbour is computed, which acts as the u^+ . This operation is done for every pair of common edges. Another concern is truncation of the outer boundaries of the computational domain. For scattering problems in particular, we require that the scattered field dampens as it moves sufficiently far away from the scatterer to safely truncate the domain [4]. To achieve this, the domain is padded with a perfectly matched layer (PML) along the outer boundaries such that they do not produce spurious oscillations at their interface with the inner domain [15].

4 Divergence Error

4.1 Dependence of divergence on discretization

In the absence of dedicated divergence constraint preserving methods, numerical solutions to the time-domain Maxwell’s equations using conventional finite volume/finite element methods usually show small values of divergence that can be seen more as numerical artefacts [16]. In [12], Cioni et. al. showed that the finite volume method used with unstructured meshes, did not conserve exactly the divergence conditions and that the divergence error thus obtained, showed a strong dependence on the underlying discretization. The method presented, was used to solve the Maxwell’s equations to obtain a time-dependent scattered field when an object is illuminated by an incident plane wave. The L_∞ divergence error norms were shown declining with reducing mesh size and rising accuracy of the numerical scheme. A similar trend can be found in the data presented in [7]. Cockburn et. al. developed a locally divergence-free discontinuous Galerkin method therein to solve the time-domain Maxwell’s equations. The standard

and the locally divergence-free methods were compared in terms of the error norms of the solution and the divergence obtained. The error norms tabulated for the case of the advection of a smooth TM wave, shows that the divergence error fell both as the mesh size dropped and order of the basis polynomials rose. The same is verified by us although the results are not presented here, they being identical to those obtained in [7].

Despite the divergence errors, the solution and desired physical quantities show expected accuracies. For example, in the same paper [7] by Cockburn et. al., it can also be observed that the error norms of the solution do not differ significantly despite there being lower divergence error, compared to the standard method. This again is verified by us without repeating the results here. Following up with [12], Cioni et. al. used a mixed finite volume/finite element method, not accounting for the divergence constraints explicitly. They observed that the divergence errors did not distort the radar cross section(RCS) obtained and concluded that the divergence error did not have a significant influence on the higher order accurate solution. To summarize, this suggests that divergence error in higher order conservative finite volume method does show a dependence on the discretization but has an insignificant influence on the formal accuracy of the solution, especially for higher order methods. With no particular incentive from a numerics standpoint, the motivation to eliminate the divergence error comes more prominently from the physics to be captured in higher order solutions of the time domain Maxwell's equations. In magnetohydrodynamics for instance, Brackbill and Barnes [17] showed that nonzero numerical divergence causes unphysical fluid velocities, parallel to the magnetic field vector. Also, in applications such as those in magnetohydrodynamics, it is regular practice to ensure that the divergence constraints are met [18, 19, 20].

4.2 Relation between relative divergence and relative truncation errors

We observe that the Gauss' law relations, $\nabla \cdot \mathbf{B} = 0$ and $\nabla \cdot \mathbf{D} = 0$ (in free space), are not part of the evolution eqs. (1) and (2). According to the evolution equations in their continuous form, divergence of the field variables \mathbf{B} and \mathbf{E} is time independent. Therefore, if initially this divergence is zero, it will remain zero. Thus, the Gauss' law is not a dynamical condition on variables \mathbf{B} and \mathbf{E} , rather a constraint on the initial conditions. Therefore, the fact that the Gauss' law is satisfied in the continuous case, is a consequence of the evolution equations eqs. (1) and (2), coupled with appropriate initial conditions [16]. While formulating numerical methods to solve the time domain Maxwell's equations, satisfying the divergence constraint is theoretically shown to be a consequence of the curl equations and are considered redundant, if satisfied initially [12, 21]. Thus, with numerical methods approximating only the evolution equations, the differential property that the divergence is rigorously independent of time, is generally not preserved [16]. With numerical tests showing a dependence of divergence error on the discretization, in this section we establish it formally.

Consider a subsystem of the TM_z eq. (1) with (2), consisting of only in-plane components B_x and B_y , such that

$$\tilde{\mathbf{U}} = \begin{pmatrix} B_x \\ B_y \end{pmatrix} = \mathbf{B}, \quad \tilde{\mathbf{F}} = \begin{pmatrix} 0 \\ -D_z/\epsilon \end{pmatrix} \hat{i}, \quad \tilde{\mathbf{G}} = \begin{pmatrix} D_z/\epsilon \\ 0 \end{pmatrix} \hat{j}, \quad (9)$$

with $\mathbf{S} = 0$ for simplicity, and \hat{i}, \hat{j} being unit vectors along the $+x$ and $+y$ directions respectively. Conservation form for this subsystem can then be written in Cartesian co-ordinates as,

$$\frac{\partial \mathbf{B}}{\partial t} + \nabla \cdot \mathcal{F} = \frac{\partial \mathbf{B}}{\partial t} + \frac{\partial \tilde{\mathbf{F}}}{\partial x} + \frac{\partial \tilde{\mathbf{G}}}{\partial y} = 0, \quad (10)$$

where the flux is given as

$$\mathcal{F} = [\tilde{\mathbf{F}}, \tilde{\mathbf{G}}].$$

Writing the vector equation eq. (10) component-wise,

$$\frac{\partial}{\partial t} \begin{pmatrix} B_x \\ B_y \end{pmatrix} + \frac{\partial}{\partial x} \begin{pmatrix} 0 \\ -D_z/\epsilon \end{pmatrix} + \frac{\partial}{\partial y} \begin{pmatrix} D_z/\epsilon \\ 0 \end{pmatrix} = 0. \quad (11)$$

$$\frac{\partial}{\partial t} \begin{pmatrix} B_x \\ B_y \end{pmatrix} + \begin{pmatrix} \frac{\partial D_z/\epsilon}{\partial y} \\ -\frac{\partial D_z/\epsilon}{\partial x} \end{pmatrix} = 0. \quad (12)$$

Various numerical methods can be used to obtain a semi-discrete formulation of eq. (12), resulting in an explicit time-marching algorithm. An abstraction of the right hand side \mathbf{R} of the ODE thus obtained, discretized on a mesh parameterized by a size h , and spatial operators p -th order accurate, is given by

$$\frac{d\mathbf{B}_{h,p}}{dt} = \begin{pmatrix} -\frac{\partial D_z/\epsilon}{\partial y} \\ \frac{\partial D_z/\epsilon}{\partial x} \end{pmatrix}_{h,p} = \mathbf{R}_{h,p}. \quad (13a)$$

Another approximation with q -th order spatially accurate operators on the same mesh, denoted by the pair (h, q) can be formed,

$$\frac{d\mathbf{B}_{h,q}}{dt} = \mathbf{R}_{h,q}. \quad (13b)$$

Taking the divergence and then difference of eqs. (13) yields

$$\frac{d(\nabla \cdot \mathbf{B}_{h,p} - \nabla \cdot \mathbf{B}_{h,q})}{dt} = \nabla \cdot (\mathbf{R}_{h,p} - \mathbf{R}_{h,q}). \quad (14)$$

The right hand side of the eq. (14) is the divergence of the relative truncation error between the p -th and q -th order accurate discretizations on a mesh h , referred to as τ_{pq} hereafter. On the same lines, we interpret the difference in

divergence obtained between the two approximations as a relative divergence error γ_{pq} . With these definitions in place, eq. (14) yields the causal relation, which in continuous form is given by

$$\boxed{\frac{d\gamma_{pq}}{dt} = \nabla \cdot \boldsymbol{\tau}_{pq}}. \quad (15)$$

Eq. (15) represents compactly a fundamental statement that the evolution of the relative divergence error is fed by the relative discretization error acting as a source. If p is taken to be infinity, *i.e.* corresponding to the continuous case, then eq. (15) suggests that it is due to the act of discretization that a divergence error is generated. The causal relation eq. (15) between the two errors, forms the rationale behind treating divergence error as a surrogate to truncation error.

A relevant simplification of the causal relation eq. (15) in the case of a plane wave, yields further insight. Consider a plane wave solution to eq. (2), restricted to a single frequency ω here, as a representative instance,

$$D_z = D_{z0} e^{(\mathbf{k} \cdot \mathbf{x} - \omega t)}, \quad (16)$$

$$B_y = -\sqrt{\frac{\mu}{\epsilon}} D_z \cos\phi, \quad (17)$$

$$B_x = \sqrt{\frac{\mu}{\epsilon}} D_z \sin\phi, \quad (18)$$

where \mathbf{x} is a position vector in the xy plane; $\mathbf{k} = \frac{\omega}{c} [\cos\phi, \sin\phi]^T$ is the wavenumber with ϕ being the angle made with the $+x$ axis. $c = \frac{1}{\sqrt{\mu\epsilon}}$ is the speed of propagation in the medium. From eq. (13a), the flux residual $\mathbf{R}_{h,p}$ for plane wave solutions, is given by

$$\mathbf{R}_{h,p} = \begin{pmatrix} -\frac{\partial D_z/\epsilon}{\partial y} \\ \frac{\partial D_z/\epsilon}{\partial x} \end{pmatrix}_{h,p} = \begin{pmatrix} \frac{\partial B_y}{\partial y} \frac{c}{\cos(\phi)} \\ \frac{\partial B_x}{\partial x} \frac{c}{\sin(\phi)} \end{pmatrix}_{h,p}. \quad (19)$$

We introduce the notation $\llbracket (\cdot) \rrbracket_{pq} := (\cdot)_{h,p} - (\cdot)_{h,q}$, used hereafter to represent the difference between quantities discretized using two levels (h, p) and (h, q) , varying in order of spatial accuracy.

The relative truncation error $\boldsymbol{\tau}_{pq}$ is therefore given by

$$\boldsymbol{\tau}_{pq} = \begin{pmatrix} \llbracket \frac{\partial B_y}{\partial y} \rrbracket_{pq} \frac{c}{\cos(\phi)} \\ \llbracket \frac{\partial B_x}{\partial x} \rrbracket_{pq} \frac{c}{\sin(\phi)} \end{pmatrix}. \quad (20)$$

By the definition of relative divergence error given earlier,

$$\gamma_{pq} = \llbracket \nabla \cdot \mathbf{B} \rrbracket_{pq} = \llbracket \frac{\partial B_x}{\partial x} \rrbracket_{pq} + \llbracket \frac{\partial B_y}{\partial y} \rrbracket_{pq}. \quad (21)$$

Eqs. (20) and (21) yield the following relation between relative divergence and relative truncation errors

$$\boxed{\gamma_{pq} = \boldsymbol{\tau}_{pq} \cdot \frac{\boldsymbol{\phi}}{c}}, \quad (22)$$

where $\boldsymbol{\phi} = [\cos \phi, \sin \phi]^T$, is a unit vector along the direction of wave travel. This simple relation institutes γ as a scalar proxy of $\boldsymbol{\tau}$. The relative divergence error is a scaled projection of the relative truncation error along the direction of travel. This is the essential link between the feature divergence, and the truncation error which facilitates its use as an indicator of truncation error. Also, since the divergence of the solution is readily available, it serves as an inexpensive driver in adaptive algorithms. A divergence error based method would naturally seem to belong to the feature-based class of adaptive algorithms, but these mutual relations make this method, essentially a truncation error-based method. The truncation and discretization error are related to each other by the Discretization Error Transport Equation (DETE), which shows that truncation error acts as a local source of discretization error [22]. This made the case for preferring truncation error as a sensor for adaptive algorithms. Hence, the extensive work in the area of truncation error estimation [22, 23, 24]. A divergence error based sensor need not rely on estimation procedures directly.

5 Numerical test of causal relationship

The causal relation between relative divergence and relative truncation errors was established as eq. (15). Its simplification for plane waves eq. (22), is numerically corroborated in this section. Two canonical problems: advection of smooth data in a rectangular domain, and scattering off a circular cylinder have been used to demonstrate that the simplified causal relation eq. (22) holds, first through a preliminary visualization and then by showing that with richer discretizations, difference between the two sides of the equation can be brought arbitrarily close to zero, thereby establishing a direct association between the two errors.

5.1 Preliminary validation

5.1.1 Advection of smooth initial data

The time domain Maxwell's equations admit the following plane wave solution [25]

$$\begin{pmatrix} H_x \\ H_y \\ E_z \end{pmatrix} = \begin{pmatrix} -\beta \\ \alpha \\ 1 \end{pmatrix} e^{(\cos(\omega t + \alpha x + \beta y))}, \quad (23)$$

where α , β and ω are constants. The computational domain Ω is taken as

$$\Omega = \left[0, \frac{2\pi}{|\omega\alpha|} \right] \times \left[0, \frac{2\pi}{|\omega\beta|} \right], \quad (24)$$

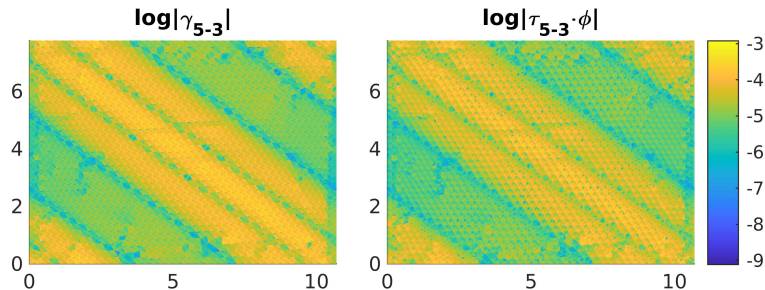


Figure 2: Validation of simplified causal relation, advection of smooth initial data

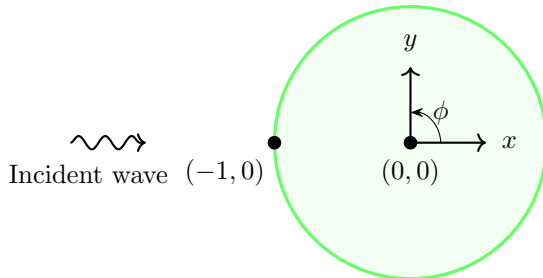


Figure 3: Schematic for the circular cylinder scattering problem

with $\omega = 1$, $\alpha = \cos(0.3\pi)$, $\beta = \sin(0.3\pi)$ and periodic boundaries.

Two instances of the problem are run, once with a uniform order of accuracy p and the other with q , for 10 periods. Post-processing involves computing the difference between relevant quantities (divergence for γ , and flux residual \mathbf{R} for τ) from the two simulations, to get γ_{pq} and τ_{pq} . A representative instance is shown in fig. 2. The left panel shows γ_{5-3} , *i.e.* the relative divergence error between discretizations with uniform $p = 5$ and another uniform $q = 3$ throughout the spatial domain. This tallies with the right panel, which shows the right side of eq. (22), $\tau_{5-3} \cdot \phi$.

5.1.2 Scattering off a circular cylinder

The next problem is of scattering off a circular cylinder under continuous illumination. An incident TM_z harmonic wave strikes a perfectly conducting cylinder of electrical size 2λ and scatters off its surface. Electrical size is defined as the number of wavelengths occupied by a characteristic length scale of the body, here, diameter of the circular cylinder. Fig. 3 shows a schematic of the problem. Given the simple geometry, a harmonic steady state is reached within 2 time periods.

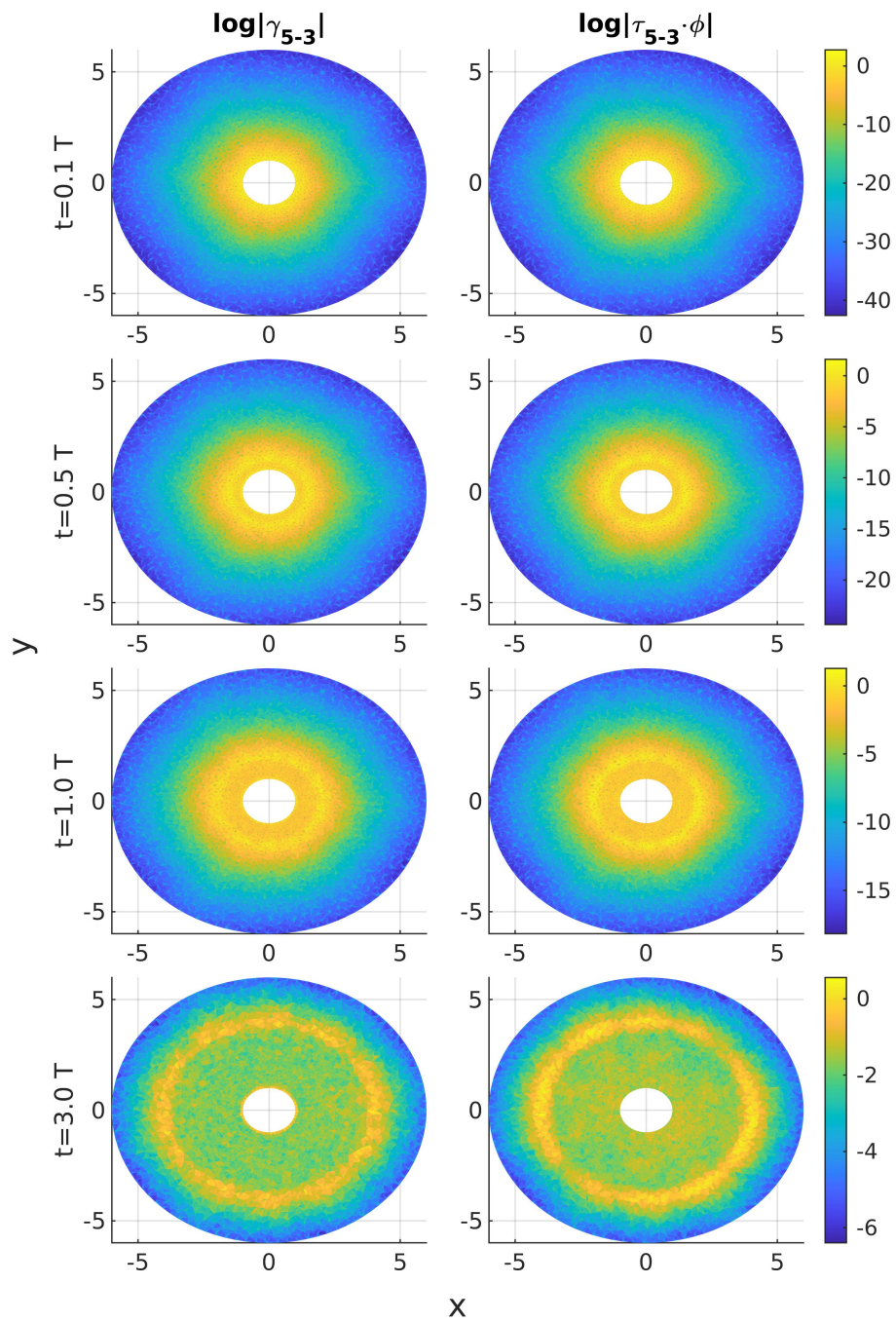


Figure 4: Validation of simplified causal relation, scattering from a circular cylinder

As done previously with the advection problem, fig. 4 compares the two sides of the simplified causal relation eq. (22), in the xy -plane at various time levels t, T denoting the time period. There is both qualitative and quantitative agreement between every pair of panels, showing evolution of the problem. The nature of the quantity γ is in close accordance with that of $\tau \cdot \phi$, as expected.

5.2 Convergence of relative errors γ_{pq} and τ_{pq}

To further this analysis, we show the behaviour of the two errors in the simplified causal relation for plane waves eq. (22), with varying discretizations. As earlier, two separate instances, a uniform order p and another with a uniform q are run, and the relative errors γ_{pq} and τ_{pq} are computed, this time at multiple regular intervals. This process is repeated for a fixed p and various values of q , and therefore multiple such simulations are run. Here, we take $p = 8$ and $q = [2, \dots, p - 1]$. L_∞ norm of the time averaged left and right sides of eq. (22) over a time period, namely γ_{8-q} and $\tau_{8-q} \cdot \phi$, are shown in fig. 5. At every node we compute a time-averaged relative quantity, then take its L_∞ norm over space. Fig. 5a shows the L_∞ norms of the time averaged γ_{8-q} and $\tau_{8-q} \cdot \phi$ for various q , for the problem of advection along a diagonal. With increasing q , as the difference $p - q$ gets lower, the relative truncation error $\tau_{8-q} \cdot \phi$ expectedly reduces and γ_{8-q} follows to convergence. A similar convergence pattern can be observed in the case of the cylinder scattering problem, the plot for which is shown in fig. 5b. Thus, as q approaches p , the relative truncation error reduces and the relative divergence error follows clearly to convergence up to $q = p - 1$. This forms the motivation to utilize local divergence error as an indicator in a p -adaptive method.

6 Algorithm

With relative divergence error identified as proxy to relative truncation error, in this section we develop a p adaptive algorithm based on divergence. This requires mapping the set of local values of divergence $\nabla \cdot \mathbf{H}_{h,p}^k$ in every element D^k , to a proposed order p_{new}^k . Note that divergence of the magnetic field vector has been taken in the TM case. Equivalently, divergence of the electric field is to be considered in the TE case. The strategy is to simply create a logarithmic mapping between the magnitudes of the divergence, and integers in the range $[1, N]$. The parameter N is a predefined maximum degree of the polynomial basis functions.

1. The divergence resulting from a discretization shows a wide spectrum of spatial scales. The input is a set of values of the divergence in an element k , at a given time level (n) for a discretization (h, p) . The objective is to come up with a new discretization (h, p_{new}) .

$$div = \left\{ \nabla \cdot \mathbf{H}_{h,p} \left(\mathbf{x}_i, t^{(n)} \right) \Big|_{D^k}; i \in [1, \dots, N_p], k \in [1, \dots, K] \right\}; \quad (25)$$

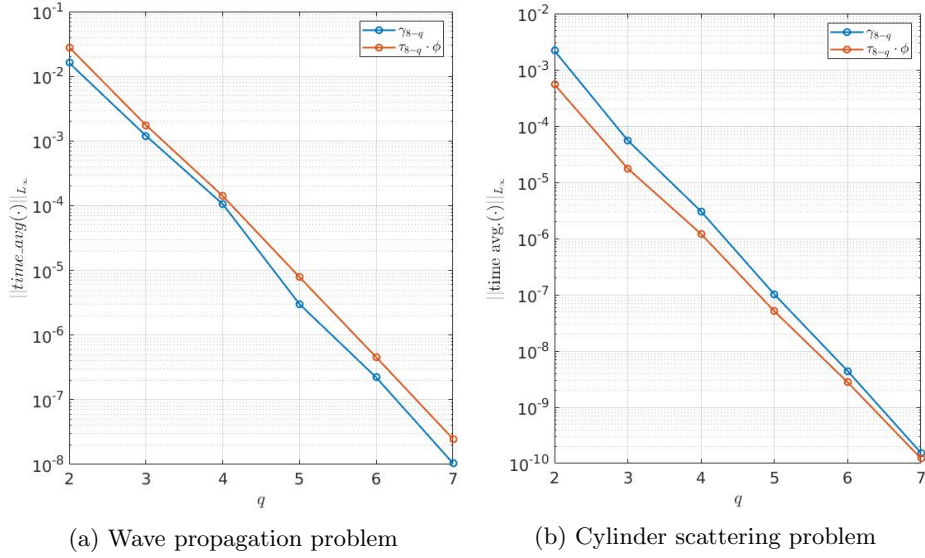


Figure 5: Convergence of time averaged L_∞ norms of γ_{8-q} and $\tau_{8-q} \cdot \phi$

div is a set of all local values of divergence of \mathbf{H} . The number of nodes N_p and hence number of values of divergence, in an element D^k , depends on the order p of the local polynomial basis functions. So, the above set is $\sum_{k=1}^K N_p(p^k)$ big, referred to as $nDOF$ in the input to algorithm 1.

2. Taking a logarithm of the absolute values of div segregates the spatial scales. This set is then shifted and scaled by a factor, to the range $[0, N]$.

$$factor : \log_{10} |div| \rightarrow ord \in [0, N] \quad (26)$$

ord is an intermediate data set, $nDOF$ in size.

3. At this stage, entries of f are real numbers. Corresponding to every element D^k , there are N_p entries in f , indexed by $i \in [1, \dots, N_p]$. We take the ceiling values of f and since there has to be a unique p_{new}^k , we pick the maximum out of these.

$$p_{new}^k = \max_{i \in [1, \dots, N_p]} \lceil f_i^k \rceil \quad (27)$$

This seems a conservative choice; the rationale behind it is that it is tracking the truncation error closely. In other words, out of all the nodes in an element demanding various p , the order of the cell, *i.e.* the one applicable on all nodes should be the maximum asked for.

4. Finally, as a sanity check, cells with all nodes having $f = 0$, are kept at the $p = 1$ level. Also, cells forming the PML boundary if employed, are kept at the $p = N$ level to avoid any spurious interactions.

The steps involved are stated concisely in algorithm 1.

Algorithm 1: p -adaptation routine, logarithmic map

Input: $\text{div} = \nabla \cdot \mathbf{H}_{h,p}^{(n)}$ or $\nabla \cdot \mathbf{E}_{h,p}^{(n)}$ *shape:* $[\text{nDOF}, 1]$
Output: p_{new} *shape:* $[K, 1]$

- 1 $\text{logdiv} = \log_{10}(\text{abs}(\text{div}))$;
- 2 $\text{shift} = -\min(\text{logdiv})$;
- 3 $\text{scale} = 1/\max(\text{logdiv}+\text{shift})$;
- 4 $\text{logdiv} = (\text{logdiv}+\text{shift})*\text{scale}$; *shift and scale to range $[0, 1]$*
- 5 $\text{ord} = \lceil N*\text{logdiv} \rceil$; *scale to $[0, N]$, take ceiling values*
- 6 $\text{i1}=0; \text{i2}=0$; *to index into ord*
- 7 **for** $k = [1, \dots, K]$ **do**
- 8 $\text{i1}=\text{i2}+1; \text{i2}=\text{i2}+N_p(p^k)$;
- 9 $p_{\text{new}}(k)=\max(\text{ord}(\text{i1}:\text{i2}))$; *take max out of $N_p(p^k)$ values*
- 10 **end**
- 11 sanity check: $p_{\text{new}}^k = 1$; $\forall k$ with $p_{\text{new}}^k = 0$
- 12 boundary/PML cells at $p = N$; $p_{\text{new}} \in \{1, \dots, N\}$

7 Results

7.1 Scattering off a circular cylinder

The proposed algorithm is applied on the cylinder scattering problem as a proof of concept. A schematic of the problem is shown in fig. 3. Variations of the problem in terms of electrical sizes and incident TM and TE illumination are presented.

The surface current at point $(-1, 0)$ as shown in the schematic fig. 3, for a cylinder 2λ in diameter under TM illumination, is plotted in fig. 6 for various $p = 1, \dots, 8$. Another instance with an adaptive routine running a combination of all levels $p = [1, \dots, 8]$ according to algorithm 1 is compared. The surface current is sinusoidal, so approximations accurate up to various orders are visibly distinguishable and suggest that a variation in p does show up in the results up to at least $p = 8$. Therefore, this is used as a suitable test case for comparison between the p -adaptive and the standard uniform p methods.

Figs. 7 and 8 show the scattering width obtained, compared to the exact solutions under TM and TE illuminations respectively, for a scatterer 2λ in size. Viewing angle 0^0 is measured from the $+x$ axis as shown in the schematic fig. 3. Here, the adaptive algorithm takes $N = 8$, *i.e.*, $p = [1, \dots, 8]$. The adaptation takes place every iteration, throughout the duration of the problem including the initial unsteady phase, followed by its evolution into a harmonically steady state.

A similar comparison for a larger scatterer of size 15λ is shown in fig. 9. As a representative illustration, fig. 10 shows the distribution of p in the domain at the one period mark. Cells forming the scattering surface and in close proximity are at $p = 8$ and it drops radially outwards. A linear variation of p in the radial direction can be seen, in accordance with algorithm 1 that created a linear

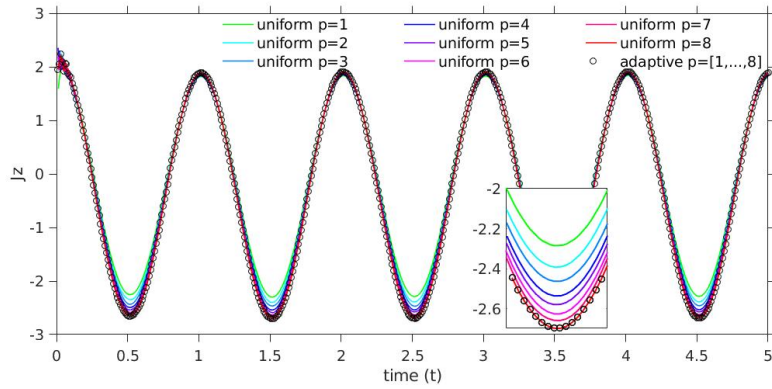


Figure 6: Surface current at $(-1,0)$ for various p , circular cylinder scattering

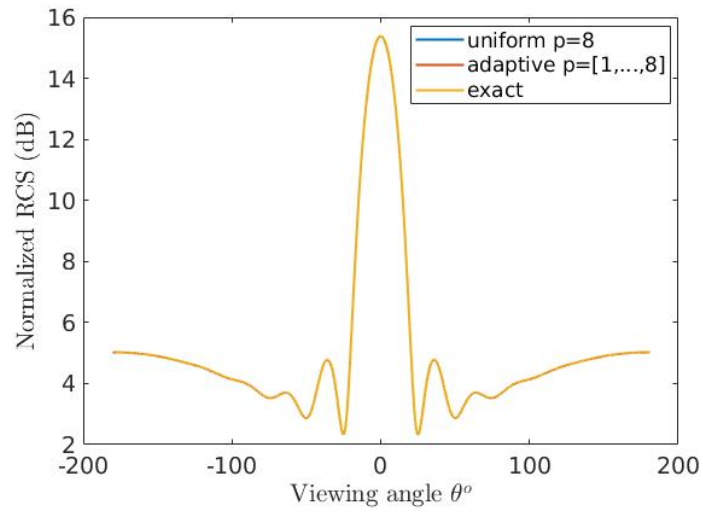


Figure 7: RCS, circular cylinder scattering, size 2λ , TM illumination

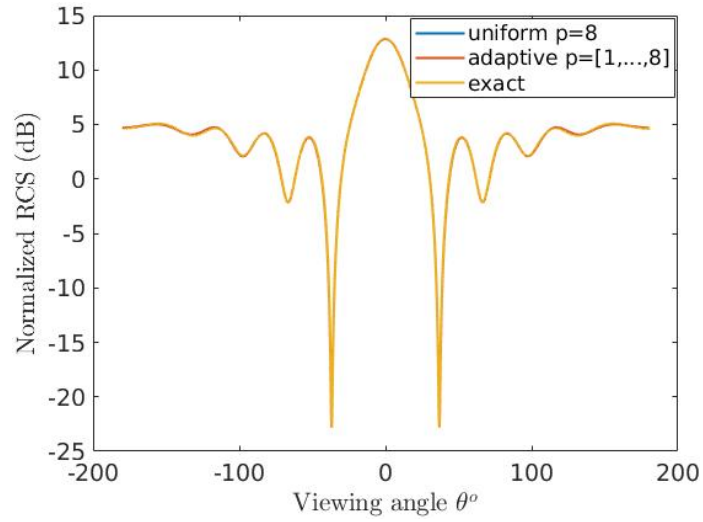


Figure 8: RCS, circular cylinder scattering, size 2λ , TE illumination

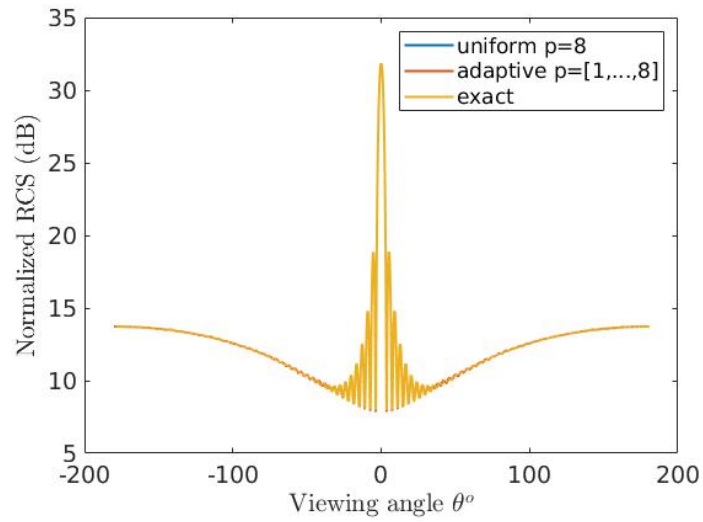


Figure 9: RCS, circular cylinder scattering, size 15λ , TM illumination

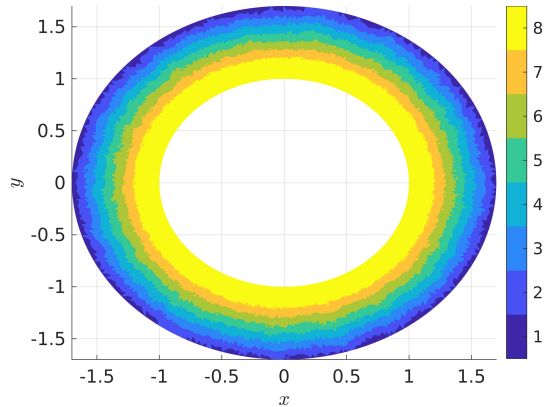


Figure 10: Distribution of p , circular cylinder scattering, size 15λ

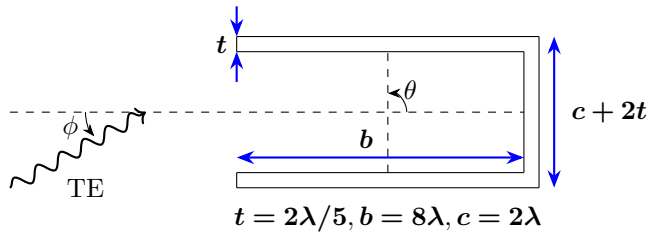


Figure 11: Schematic for the semi-open cavity problem

mapping between the order of magnitudes of local divergence of the solution, and integers $[1, \dots, N]$.

7.2 Semi-open cavity

The adaptive algorithm is next applied to scattering from a semi-open cavity. The complexity of this problem over the cylinder as a scatterer lies in the multiple internal reflections that the solution goes through in the cavity. Fig. 11 shows the schematic of the problem. A TE wave, incident at an angle ϕ to the x -axis impinges on the scatterer as shown. We present results for two such angles $\phi = 0^0, 30^0$. The computational domain is padded with a PML 1λ wide to truncate the domain. To aid visualization of the solution, fig. 12 shows H_z under TE illumination at $\phi = 0^0$. The figure compares solutions obtained from the uniform $p = 8$ and the adaptive $p = [1, \dots, 8]$ methods.

The RCS plots are also compared as in fig. 13. A 5th order accurate hybrid Galerkin solution to this problem, presented in [26] has been used as reference. Results shown have been computed at the 40 period mark, the solution being well converged.

Next, we consider $\phi = 30^0$. The H_z plots for uniform $p = 8$ and adaptive

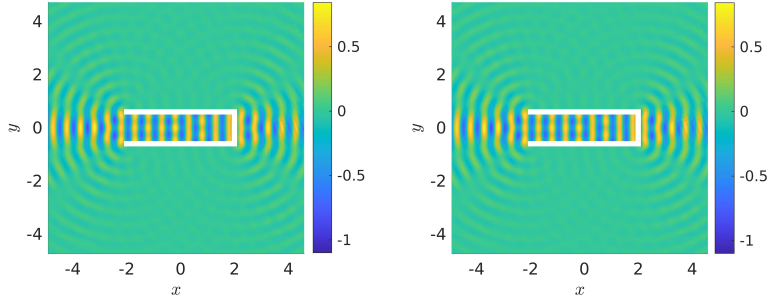


Figure 12: Scattered H_z : uniform $p = 8$ vs. adaptive $p = [1, \dots, 8]$

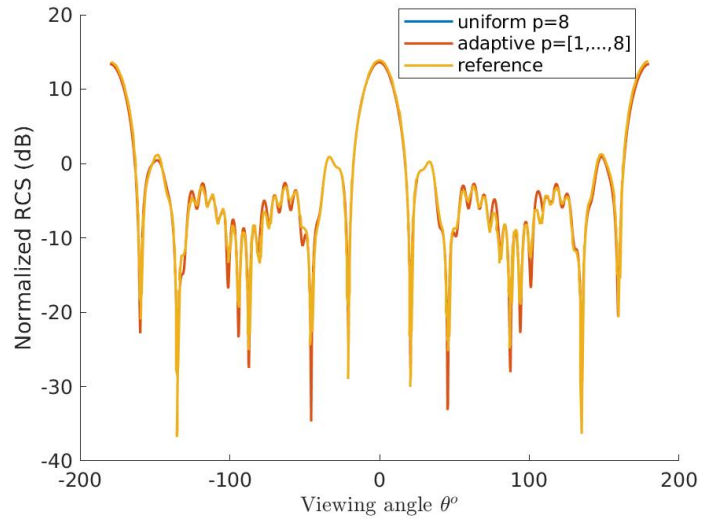


Figure 13: RCS, semi-open cavity $8\lambda \times 2\lambda$, $\phi = 0^0$

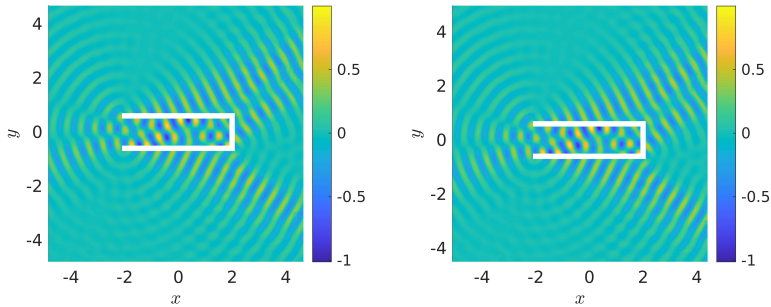


Figure 14: Scattered H_z : uniform $p = 8$ vs. adaptive $p = [1, \dots, 8]$

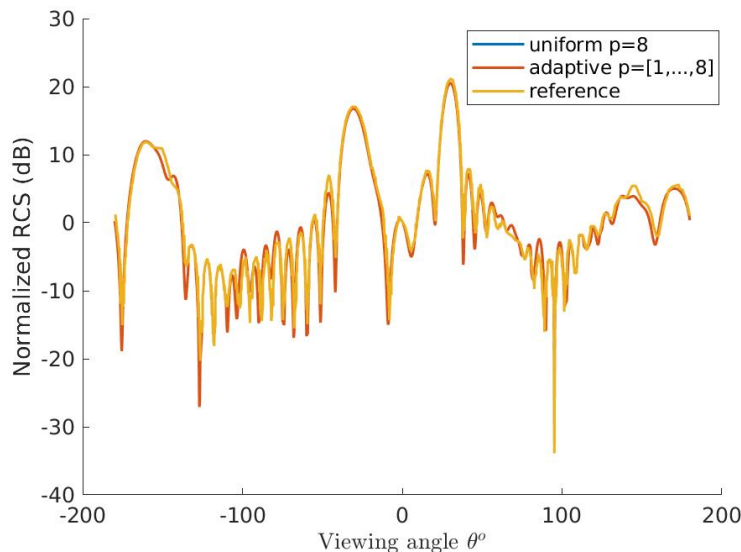


Figure 15: RCS, semi-open cavity $8\lambda \times 2\lambda$, $\phi = 30^\circ$

$p = [1, \dots, 8]$ are shown in fig. 14 and the RCS obtained, in fig. 15. The simulation takes longer to converge due to multiple internal reflections and takes up to 50 periods. The reference solution is a 8th finite element frequency domain solution from [27]. There is good agreement between the adaptive and reference solutions except the sharpness of the troughs in a few places which is usually not expected to match exactly. Also noticeable, is that the plots for the adaptive and uniform cases are indistinguishably close, which is true of all results presented further as well. Since a variable p method cannot be expected to perform any better than its uniform counterpart, it is reasonable to consider the adaptive algorithm effective.

7.3 Two adjacent cylinders

Another canonical problem to address the complexity of multiple reflections and reciprocal interactions is the that of multiple scatterers [28]. In this section, we present results for the problem of two adjacent circular cylindrical scatterers, the schematic for which is shown in fig. 16. An incident TE wave illuminates the two cylinders in the configuration shown with the angle of incidence $\phi = 270^\circ$. The scatterers are 6.4 wavelengths apart and the diameter of each of them is 4 times the wavelength of the incident wave, thus lying in the optical scattering territory.

Fig. 17 shows instantaneous scattered H_z in harmonically steady state, comparing the uniform $p = 8$ and adaptive $p = [1, \dots, 8]$ methods. They can be seen to be in accordance with each other. The corresponding RCS plots in fig. 18 are compared with a 6th order accurate hybrid Galerkin solution [26].

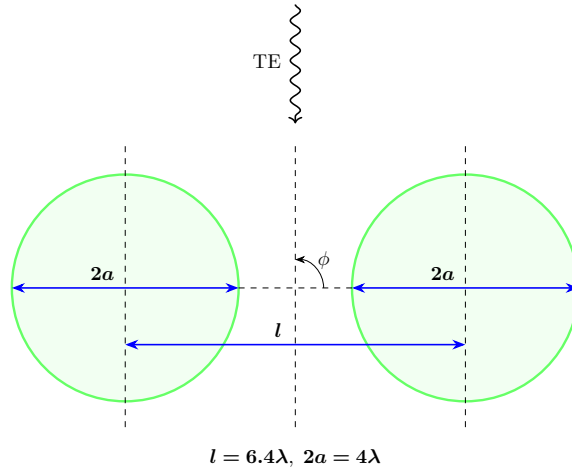


Figure 16: Schematic for the scattering off 2 adjacent cylinders problem

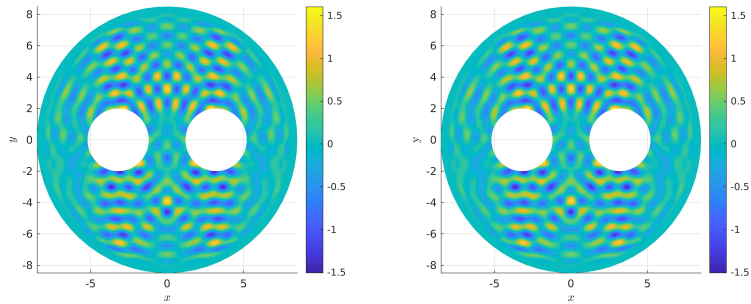


Figure 17: Scattered H_z , 2 adjacent cylinders, $\phi = 270^\circ$, uniform $p = 8$ vs. adaptive $p = [1, \dots, 8]$

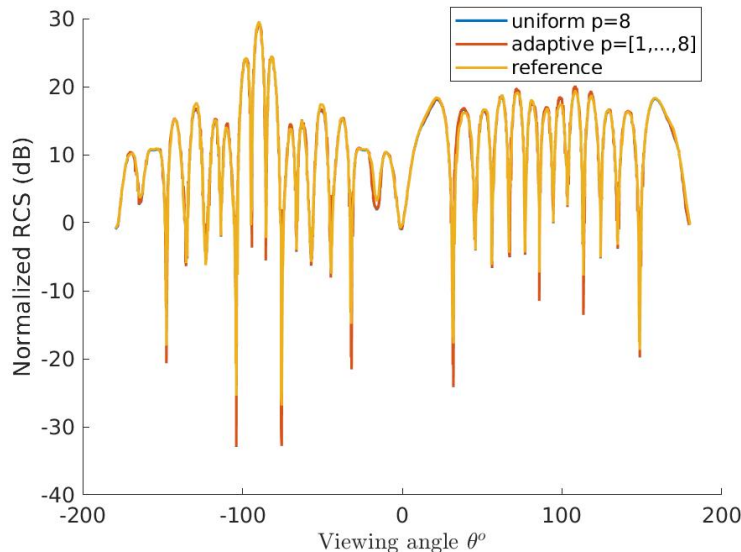


Figure 18: RCS, 2 adjacent cylinders, $\phi = 270^0$

As in the case of the semi-open cavity, the plots corresponding to the uniform and the adaptive methods are close to each other and agree with that of the reference solution.

7.4 3 adjacent cylinders

Continuing with the theme of numerous scatterers giving rise to multiple reflections off each other, the next illustration has three adjacent scatterers [29]. A schematic of the problem is shown in fig. 19. An incident TM wave strikes at an angle of incidence $\phi = 90^0$, scatterers each of circumference 0.75λ and placed one wavelength apart axially. Comparisons are made between the uniform $p = 8$ and adaptive $p = [1, \dots, 8]$ methods.

The mutual interactions can be visualized using plots of the instantaneous scattered E_z in harmonically steady state, shown in fig. 20 and match with the ones in the reference solution [30]. Fig. 21 shows the RCS plots obtained with the uniform and adaptive p methods, compared to the reference solution which is obtained analytically [29]. This set of test cases and the consistent agreement with the reference solutions, show the efficacy of the divergence driven p -adaptive algorithm proposed.

The proposed algorithm serves to introduce the philosophy of utilizing numerical divergence in such adaptive methods, as opposed to eliminating it or leaving untreated. Divergence as a quantity can be exactly computed in real time, coupled with the fact that it does not require an estimation procedure, as with traditional truncation or discretization error based techniques [31, 32, 23].

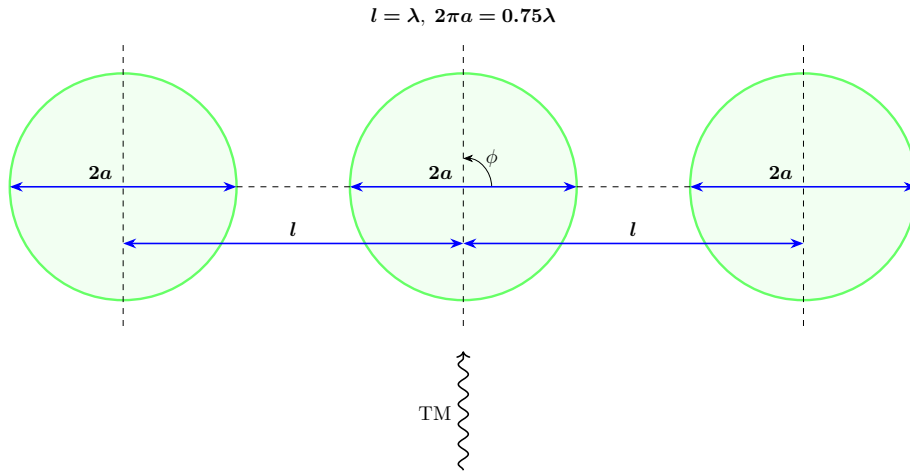


Figure 19: Schematic for the scattering off 3 adjacent cylinders problem

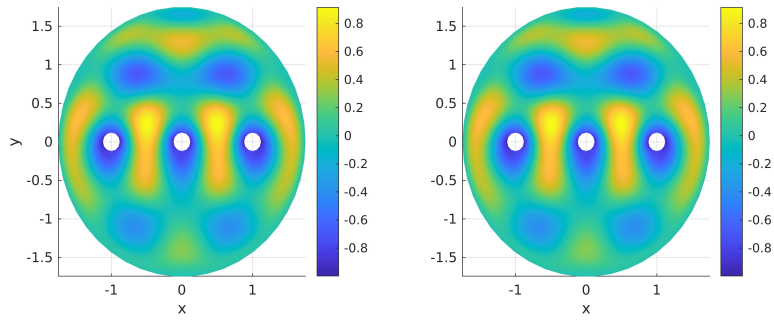


Figure 20: Scattered E_z , 3 adjacent cylinders, $\phi = 90^\circ$, uniform $p = 8$ vs. adaptive $p = [1, \dots, 8]$

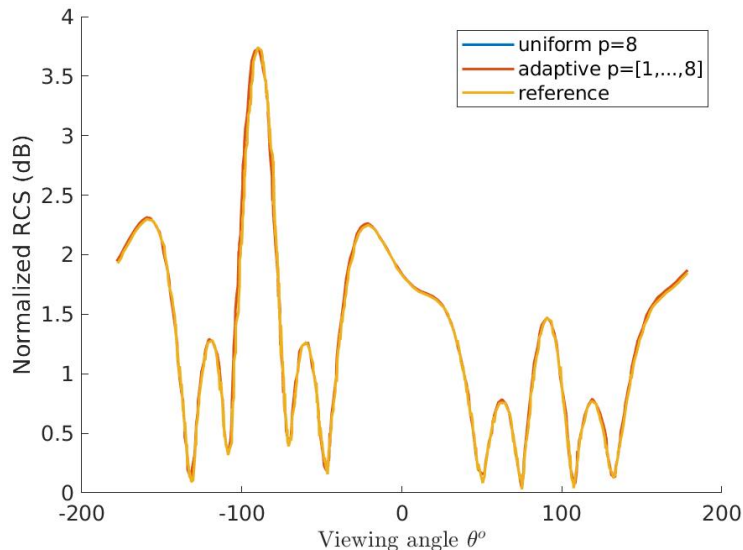


Figure 21: RCS, 2 adjacent cylinders, $\phi = 90^\circ$

Problem size, illumination	Savings in DOFs (%)	effective p
2λ , TM	43.14	5.31
2λ , TE	43.41	5.30
15λ , TM	34.36	5.90
15λ , TE	35.01	5.87

Table 1: Computational savings in DOFs and effective p employed to achieve accuracy corresponding to a uniform 8th order method.

7.5 Computational performance

In this section, we measure the computational gain obtained using the proposed divergence error driven p -adaptive method. The problem of scattering off a circular cylinder as shown in fig. 3 is used, with variations in electrical size 2λ , 15λ and the incident illumination TM, TE. The 15λ cases use a mesh two-thirds as dense as the one used in the 2λ cases on a points per wavelength basis. We compare harmonically steady p -adaptive solutions with p varying between $[1, \dots, 8]$, to a uniform $p = 8$ solution in all cases and present the savings achieved in the time averaged number of DOFs required to achieve similar accuracy. Also, an average p , averaged over both time and space, is shown in table 1 to indicate the effective p used to achieve 8th order accurate solutions.

Fig. 22 shows histograms of time-averaged p over the computational do-

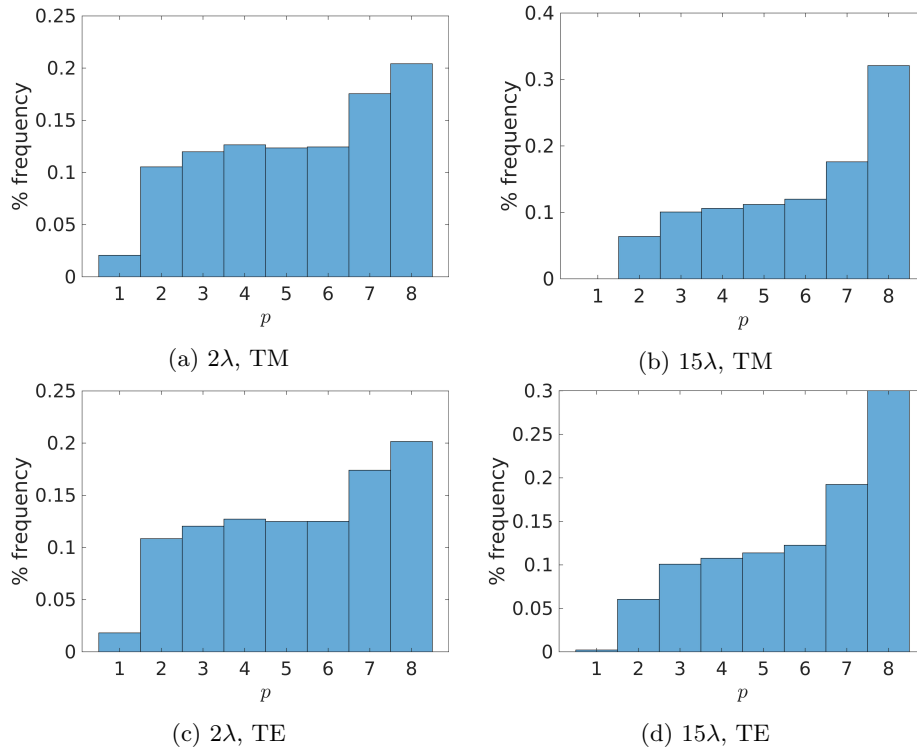


Figure 22: Histogram of time averaged p for various scatterer sizes and incident illumination in the cylinder scattering problem.

main. A larger scatterer, here the 15λ in size, naturally uses more $p = 8$ cells while expectedly the incident illumination does not affect the distribution. The savings in DOFs show the cost effectiveness of the divergence error as driver for p -adaptive methods.

8 Conclusion

A divergence driven p -adaptive method is shown to work effectively in wave dominated problems of electromagnetic scattering in DGTD methods. The proposed p -variable method is shown to be as good as a uniform p method in terms of the resulting quantities of interest. A theory with regard to divergence error is formulated and relations between relative truncation and relative divergence errors have been established analytically, supported by numerical corroboration. Illustrations using a simple p -adaptive algorithm based on the proposed theory have been presented to show the effectiveness of the divergence error, used as a driver in such algorithms.

Moreover, a novel perspective is presented in the context of treatment of the numerical divergence errors appearing in such simulations. The underutilized divergence error is shown to have potential to drive adaptive algorithms. Traditionally, these errors when present, are eliminated by modelling the system to closely satisfy the divergence constraints or making dedicated effort to clean them explicitly. It is also common to not eliminate the divergence errors, where their presence may not deteriorate either the solution or the objective functionals. Extending this discussion, it is shown that there is an opportunity to utilize the divergence error to computational gain, at the algorithm layer.

References

- [1] Kane Yee. “Numerical solution of initial boundary value problems involving maxwell’s equations in isotropic media”. In: *IEEE Trans. Antennas Propag.* 14.3 (1966), pp. 302–307. ISSN: 0018-926X. DOI: [10.1109/TAP.1966.1138693](https://doi.org/10.1109/TAP.1966.1138693). URL: <http://ieeexplore.ieee.org/document/1138693/>.
- [2] Susan C Hagness, Allen Taflove, and Stephen D Gedney. “Finite-Difference Time-Domain Methods”. In: *Handb. Numer. Anal.* Vol. 13. 04. 2005, pp. 199–315. ISBN: 9780444513755. DOI: [10.1016/S1570-8659\(04\)13003-2](https://doi.org/10.1016/S1570-8659(04)13003-2). URL: <https://linkinghub.elsevier.com/retrieve/pii/S1570865904130032>.
- [3] Vijaya Shankar, Alireza H. Mohammadian, and William F. Hall. “A Time-Domain, Finite-Volume Treatment for the Maxwell Equations”. In: *Electromagnetics* 10.1-2 (1990), pp. 127–145. ISSN: 1532527X. DOI: <https://doi.org/10.1080/02726349008908232>. URL: <https://doi.org/10.1080/02726349008908232>.
- [4] Jan S. Hesthaven and Tim Warburton. *Nodal Discontinuous Galerkin Methods*. Vol. 54. Texts in Applied Mathematics. New York, NY: Springer New York, 2008. ISBN: 978-0-387-72065-4. DOI: [10.1007/978-0-387-72067-8](https://doi.org/10.1007/978-0-387-72067-8). URL: <http://link.springer.com/10.1007/978-0-387-72067-8>.
- [5] F. Assous et al. “On a Finite-Element Method for Solving the Three-Dimensional Maxwell Equations”. In: *J. Comput. Phys.* 109.2 (1993), pp. 222–237. ISSN: 00219991. DOI: [10.1006/jcph.1993.1214](https://doi.org/10.1006/jcph.1993.1214).
- [6] C.-D. Munz et al. “Divergence Correction Techniques for Maxwell Solvers Based on a Hyperbolic Model”. In: *J. Comput. Phys.* 161.2 (2000), pp. 484–511. ISSN: 00219991. DOI: [10.1006/jcph.2000.6507](https://doi.org/10.1006/jcph.2000.6507). URL: <https://www.sciencedirect.com/science/article/pii/S0021999100965070>.
- [7] Bernardo Cockburn, Fengyan Li, and Chi Wang Shu. “Locally divergence-free discontinuous Galerkin methods for the Maxwell equations”. In: *J. Comput. Phys.* 194.2 (2004), pp. 588–610. ISSN: 00219991. DOI: [10.1016/j.jcp.2003.09.007](https://doi.org/10.1016/j.jcp.2003.09.007).

- [8] Fengyan Li and Chi Wang Shu. “Locally divergence-free discontinuous Galerkin methods for MHD equations”. In: *J. Sci. Comput.* 22-23. June (2005), pp. 413–442. ISSN: 08857474. DOI: [10.1007/s10915-004-4146-4](https://doi.org/10.1007/s10915-004-4146-4).
- [9] Praveen Chandrashekar. “A Global Divergence Conforming DG Method for Hyperbolic Conservation Laws with Divergence Constraint”. In: *J. Sci. Comput.* 79.1 (2019), pp. 79–102. ISSN: 08857474. DOI: [10.1007/s10915-018-0841-4](https://doi.org/10.1007/s10915-018-0841-4). URL: <https://doi.org/10.1007/s10915-018-0841-4>.
- [10] Fengyan Li, Liwei Xu, and Sergey Yakovlev. “Central discontinuous Galerkin methods for ideal MHD equations with the exactly divergence-free magnetic field”. In: *J. Comput. Phys.* 230.12 (2011), pp. 4828–4847. ISSN: 10902716. DOI: [10.1016/j.jcp.2011.03.006](https://doi.org/10.1016/j.jcp.2011.03.006). URL: <http://dx.doi.org/10.1016/j.jcp.2011.03.006>.
- [11] Fengyan Li and Liwei Xu. “Arbitrary order exactly divergence-free central discontinuous Galerkin methods for ideal MHD equations”. In: *J. Comput. Phys.* 231.6 (2012), pp. 2655–2675. ISSN: 10902716. DOI: [10.1016/j.jcp.2011.12.016](https://doi.org/10.1016/j.jcp.2011.12.016). URL: <http://dx.doi.org/10.1016/j.jcp.2011.12.016>.
- [12] J.P. Cioni, Loula Fezoui, and Herve Steve. “A Parallel Time-Domain Maxwell Solver Using Upwind Schemes and Triangular Meshes”. In: *IMPACT Comput. Sci. Eng.* 5.3 (1993), pp. 215–247. ISSN: 08998248. DOI: [10.1006/icse.1993.1010](https://doi.org/10.1006/icse.1993.1010). URL: <https://linkinghub.elsevier.com/retrieve/pii/S0899824883710104>.
- [13] Avijit Chatterjee. “A Multilevel Numerical Approach with Application in Time-Domain Electromagnetics”. In: *Commun. Comput. Phys.* 17.3 (2015), pp. 703–720. ISSN: 1815-2406. DOI: [10.4208/cicp.181113.271114a](https://doi.org/10.4208/cicp.181113.271114a). URL: <https://www.cambridge.org/core/product/identifier/S1815240615000158/type/journal-article>.
- [14] D Moxey et al. “Towards p-Adaptive Spectral/hp Element Methods for Modelling Industrial Flows”. In: *Spectr. High Order Methods Partial Differ. Equations ICOSAHOM 2016*. Ed. by Marco L Bittencourt, Ney A Dumont, and Jan S Hesthaven. Cham: Springer International Publishing, 2017, pp. 63–79. ISBN: 978-3-319-65870-4.
- [15] Saul Abarbanel and David Gottlieb. “On the construction and analysis of absorbing layers in CEM”. In: *Appl. Numer. Math.* 27.4 (1998), pp. 331–340. ISSN: 01689274. DOI: [10.1016/S0168-9274\(98\)00018-X](https://doi.org/10.1016/S0168-9274(98)00018-X).
- [16] John D. Ramshaw. “A method for enforcing the solenoidal condition on magnetic field in numerical calculations”. In: *J. Comput. Phys.* 52.3 (1983), pp. 592–596. ISSN: 00219991. DOI: [10.1016/0021-9991\(83\)90009-8](https://doi.org/10.1016/0021-9991(83)90009-8). URL: <https://linkinghub.elsevier.com/retrieve/pii/S0021999183900098>.

- [17] J.U Brackbill and D.C Barnes. “The Effect of Nonzero $\nabla \mathbf{b} \cdot \mathbf{B}$ on the numerical solution of the magnetohydrodynamic equations”. In: *J. Comput. Phys.* 35.3 (1980), pp. 426–430. ISSN: 00219991. DOI: [10.1016/0021-9991\(80\)90079-0](https://doi.org/10.1016/0021-9991(80)90079-0). URL: <https://linkinghub.elsevier.com/retrieve/pii/0021999180900790>.
- [18] Christoph Altmann et al. “A local time-stepping Discontinuous Galerkin algorithm for the MHD system”. In: *ESAIM Proc.* 28.August (2009), pp. 33–54. ISSN: 2267-3059. DOI: [10.1051/proc/2009038](https://doi.org/10.1051/proc/2009038).
- [19] V. Wheatley, H. Kumar, and P. Huguenot. “On the role of Riemann solvers in Discontinuous Galerkin methods for magnetohydrodynamics”. In: *J. Comput. Phys.* 229.3 (2010), pp. 660–680. ISSN: 00219991. DOI: [10.1016/j.jcp.2009.10.003](https://doi.org/10.1016/j.jcp.2009.10.003).
- [20] S. Naranjo Alvarez et al. “The virtual element method for resistive magnetohydrodynamics”. In: *Comput. Methods Appl. Mech. Eng.* 381 (2021), p. 113815. ISSN: 00457825. DOI: [10.1016/j.cma.2021.113815](https://doi.org/10.1016/j.cma.2021.113815). arXiv: [2004.11467](https://arxiv.org/abs/2004.11467). URL: <https://doi.org/10.1016/j.cma.2021.113815>.
- [21] Allen Taflove and Susan C. Hagness. *Computational Electrodynamics: The Finite-Difference Time-Domain Method*. 2nd. Artech House. ISBN: 1-58053-076-1.
- [22] Moritz Kompenhans et al. “Comparisons of p-adaptation strategies based on truncation- and discretisation-errors for high order discontinuous Galerkin methods”. In: *Comput. Fluids* 139 (2016), pp. 36–46. ISSN: 00457930. DOI: [10.1016/j.compfluid.2016.03.026](https://doi.org/10.1016/j.compfluid.2016.03.026). URL: <https://linkinghub.elsevier.com/retrieve/pii/S0045793016300895>.
- [23] Andrés M. Rueda-Ramírez et al. *Truncation Error Estimation in the p-Anisotropic Discontinuous Galerkin Spectral Element Method*. Vol. 78. 1. Springer US, 2019, pp. 433–466. ISBN: 1091501807. DOI: [10.1007/s10915-018-0772-0](https://doi.org/10.1007/s10915-018-0772-0). URL: <https://doi.org/10.1007/s10915-018-0772-0>.
- [24] Alexandros Syrakos et al. “Numerical experiments on the efficiency of local grid refinement based on truncation error estimates”. In: *J. Comput. Phys.* 231.20 (2012), pp. 6725–6753. ISSN: 00219991. DOI: [10.1016/j.jcp.2012.06.023](https://doi.org/10.1016/j.jcp.2012.06.023). arXiv: [1508.02345](https://arxiv.org/abs/1508.02345). URL: <http://dx.doi.org/10.1016/j.jcp.2012.06.023>.
- [25] Bernardo Cockburn, George E. Karniadakis, and Chi-Wang Shu. *Discontinuous Galerkin Methods*. Springer-Verlag. ISBN: 978-3-642-64098-8.
- [26] R. W. Davies, K. Morgan, and O. Hassan. “A high order hybrid finite element method applied to the solution of electromagnetic wave scattering problems in the time domain”. In: *Comput. Mech.* 44.3 (2009), pp. 321–331. ISSN: 01787675. DOI: [10.1007/s00466-009-0377-4](https://doi.org/10.1007/s00466-009-0377-4).
- [27] P. D. Ledger et al. “Arbitrary order edge elements for electromagnetic scattering simulations using hybrid meshes and a PML”. In: *Int. J. Numer. Methods Eng.* 55.3 (2002), pp. 339–358. ISSN: 00295981. DOI: [10.1002/nme.501](https://doi.org/10.1002/nme.501).

- [28] J. W. Young and J. C. Bertrand. “Multiple scattering by two cylinders”. In: *J. Acoust. Soc. Am.* 58.6 (1975), pp. 1190–1195. ISSN: NA. DOI: [10.1121/1.380792](https://doi.org/10.1121/1.380792).
- [29] H. A. Ragheb and M. Hamid. “Scattering by n parallel conducting circular cylinders”. In: *Int. J. Electron.* 59.4 (1985), pp. 407–421. ISSN: 13623060. DOI: [10.1080/00207218508920712](https://doi.org/10.1080/00207218508920712).
- [30] Vaibhav Shah. “Mixed Formulation for Perfect Electric Conducting Scatterers”. PhD thesis. Indian Institute of Technology Bombay, 2021.
- [31] Christopher Roy. “Review of Discretization Error Estimators in Scientific Computing”. In: *48th AIAA Aerosp. Sci. Meet. Incl. New Horizons Forum Aerosp. Expo.* January. 2010, pp. 1–29. ISBN: 978-1-60086-959-4. DOI: [10.2514/6.2010-126](https://doi.org/10.2514/6.2010-126). URL: <http://arc.aiaa.org/doi/10.2514/6.2010-126>.
- [32] Vít Dolejší, Filip Roskovec, and Miloslav Vlasák. “Residual based error estimates for the space-time discontinuous Galerkin method applied to the compressible flows”. In: *Comput. Fluids* 117 (2015), pp. 304–324. ISSN: 00457930. DOI: [10.1016/j.compfluid.2015.05.027](https://doi.org/10.1016/j.compfluid.2015.05.027).